 CMES, vol.18, no.1, pp.17-30, 2007

Design Optimization of the Intake of a Small-Scale Turbojet Engine

R. Amirante[1], L.A. Catalano[2], A. Dadone[1] and V.S.E. Daloiso[1]

Abstract: This paper proposes a gradient-based progressive optimization technique, which can be efficiently combined with black-box simulation codes. Its efficiency relies on the simultaneous convergence of the flow solution, of the gradient evaluation, and of the design update, as well as on the use of progressively finer grids. The developed numerical technique has general validity and is here applied to the fluid-dynamic design optimization of the intake of a small-size turbojet engine, at high load and zero flight speed. Two simplified design criteria are proposed, which avoid simulating the flow in any turbojet components other than the intake itself. Using a geometrically constrained polynomial profile, both design optimizations have been produced in less than the amount of computational work to perform nine flow analyses; moreover, both optimizations have provided almost coincident intake profiles. Negligible performance improvements have been obtained by removing one geometrical constraint, at the price of almost tripling the CPU time required. Finally, the original and the optimal profiles have been mounted on the same small-scale turbojet engine and experimentally tested, to assess the resulting improvements in terms of overall performances. All numerical and experimental achievements can be extended to the intake of a microturbine for electricity generation.

Keyword: Design optimization, Finite-Difference Progressive optimization, microturbine intake.

[1] Dipartimento di Ingegneria Meccanica e Gestionale, Politecnico di Bari, Bari, Italy

[2] Contact author. DIMEG-Sezione Macchine ed Energetica, CEMeC, Politecnico di Bari, Bari, Italy. E-mail: catalano@poliba.it

1 Introduction

In the last decade, the interest in microturbines and their industrial employment have significantly grown up thanks to the very high power/weight ratio, to the small environmental impact and to the potentialities of achieving high efficiencies. In particular, this recent development responds to the need for reliable and environmentally friendly electricity generators for the new markets provided by the deregulation [Carno (1998)]. Indeed, applications involving electric power ranging from 20÷80 kW to 1 MW are considered as routine applications requiring simple and inexpensive plants and characterized by low pollutant emissions, especially low *NOx* emissions.

Meanwhile, the use of microturbines in both civil and military aeronautic and aerospace applications has become more and more attractive: microturbines have been already employed for power generation in small radio-controlled spotter planes, in the spy-rockets and in the *MIAI Abrams* tanks as auxiliary power generators. More recently, the development of unmanned aerial vehicles (UAVs) has increased the interest for small turbojet engines [Carno (1998)] derived from turbocharger rotor components. A small-scale turbojet engine can also be employed as gas generator core for small ramjet engines, powering supersonic UAVs. For both applications, *i.e.*, for small portable power generation systems and for mini or micro UAVs, the potentially very high power density of the gas turbine allows a strong reduction in battery, and thus of the overall system weight [Decuyepere and Verstraete (2005), Fernandez-Pello (2005), Guidez, Ribaud, Dessornes, and Dumand (2004), Hendrik, Verstraete and De Bruyn (2004)].

In order to be competitive with large-scale gas turbines and reciprocating engines, the microtur-

bines should offer comparable thermal efficiency. The most common strategy to improve efficiency is to preheat the inlet air to the combustor in a recuperator using the exhaust heat [Watts (1999), Hamilton (1999)]. Obviously, the reduced dimensions give rise to specific problems which have been addressed in the literature, where some criteria involved in the design of heat recuperators can be found [Jacobson (1998), Rodgers (1999) Rodgers (1997), McDonald (1996)]. Furthermore, a careful design of microturbine components can significantly increase the thermal (or conversion) efficiency. Therefore, robust but relatively simple design methodologies are needed, in order to improve the competitiveness of these small-scale equipments, while reducing their design costs. In this context, the automatic design of microturbines employing CFD and optimization techniques has attracted the interest of many researchers. This is also due to the possibility of exploring the effects of the scale reduction with respect to the standard turbine plants, *e.g.*, the combustion chamber is considered in Jacobson (1998) and Waitz, Gauba and Tzeng, (1998), while Guidez, Dumand, Courvoisier and Orain (2005) explore the lower Reynolds number effects, the high level of external heat losses and the tip clearance controlling. Guidez, Dumand, Courvoisier and Orain (2005) also simulate the behaviour of different parts of the entire plant, *i.e.*, the centrifugal compressor, the combustion chamber, the turbine.

In this paper we are concerned with the intake of microturbines for either electricity generation or propulsion, because its improved design can influence the fluid-dynamic behaviour of the other components and the overall efficiency. In particular, the intake of the Pegasus small-scale turbojet engine, produced by AMV (Amsterdam, The Netherlands), has been here considered and numerically analyzed to verify the boundary layer growth and the velocity profile at the inducer inlet. As previously underlined, the small scale and the simplicity of the microturbine under investigation do not justify complex and expensive design efforts. Therefore, the presence of the rotor blades and the shaft rotation have been neglected, so that the turbulent flow in an axisymmetric nozzle has been computed, using the CFD code Fluent [Fluent 6.1 Inc. (2003)]. The computed flow-field shows a wide recirculation zone at the inducer inlet, spanning almost 8% of the inducer inlet section. This result suggests that the intake profile can be more properly designed, with the aims of reducing the fluid-dynamic losses, improving the velocity profile at the inducer inlet and increasing the flow rate.

A trial and error approach, often used in the industrial environment, requires large amounts of computer time and man-power, and may not lead to a full optimization. Many recent contributions are available, which regard the development of design optimization methods for turbojet components and for entire aircraft configurations: P 'ascoa, Mendes, Gato and Elder (2004) propose a numerical procedure which allows to recover the blade geometry that gives the desired aerodynamic blade load distribution by relating the axial distribution of the mean tangential velocity component through the cascade with the blade camber-line angle. Morino, Bernardini and Mastroddi (2006) have recently developed a multi-disciplinary optimization method for the conceptual design of innovative aircraft configurations, based on the integrated modeling of structures, aerodynamics, and aeroelasticity. Both methods require the availability of the source files of the analysis codes. For such a reason, an alternative, efficient, automatic optimization strategy that can be used in conjunction with a black-box commercial code is needed. Genetic algorithms are unaffordable, because they require many flow analyses, even using optimal mesh partitioning and float-encoded genetic algorithms [Rama Mohan Rao, Appa Rao and Dattaguru (2004)]. An alternative approach, that can be combined with black-box commercial codes, has been recently proposed by Poloni, Giurgevich, Onesti, and Pediroda (2000): a genetic algorithm is used only for few generations to start the optimization process; then, a gradient-based technique is used, the sensitivity derivatives being evaluated by means of a properly trained neural network. The proposed method is rather complex

and still expensive, because it requires the amount of computational time to perform many configuration simulations. Dadone and Grossman (2000) have recently proposed a more efficient technique, named *progressive optimization*, which is capable of performing a complete design optimization in the amount of computational work to perform few flow analyses. However, the adjoint method of Dadone and Grossman (2000) does not allow the use of black-box analysis codes, since the source code needed to derive the adjoint system is not available. Incidentally, even if the source code were available, the derivation of the adjoint system would be very cumbersome for equations including turbulence.

In order to overcome these limits, the present paper introduces a gradient-based progressive optimization procedure, which can be simply and efficiently combined with commercial black-box simulation codes. The efficiency of the proposed optimization procedure relies on the simultaneous convergence of the flow solution, of the gradient evaluation and of the design update, as well as on the use of progressively finer grids. Hence, the solution accuracy increases while approaching the optimum and the initial configurations can be optimized at a very low computational cost.

The design optimization of the intake of the Pegasus small-scale turbojet engine is approached as a single-point optimization problem. Nevertheless, experimental results will demonstrate that similar improvement performances are obtained over the entire working range. The entire procedure could be reformulated as a multi-point optimization problem by employing the auto-adjusting weighted object optimization proposed by Zhu, Liu, Wang and Yu (2004).

First, Section 1 provides a brief description of the Pegasus small-scale turbojet engine and the numerical simulation of the flow field in the existing intake. Then, Section 2 describes the proposed gradient-based optimization procedure for black-box analysis codes, which is validated in Section 3, by means of an inverse design application. Furthermore, Section 3 presents the direct design optimization of the intake profile by employing two different objective functions. The resulting optimal profiles, some details of the corresponding flow fields, and a demonstration of the computational efficiency are provided. Finally, Section 4 describes the experimental rig employed to test the turbojet engine, and compares the overall measured performances of the reference intake with the optimized intake performances.

2 Flow analysis of the Pegasus turbojet engine intake

The Pegasus small-scale turbojet engine produced by AMV (Amsterdam, The Netherlands) is composed by the intake, a single-stage centrifugal compressor, with a radial and an axial diffuser, an annular combustion chamber, a single-stage axial turbine and a convergent exhaust nozzle.

This paper considers only the first component of the Pegasus engine, with the aim of analyzing the influence of the nozzle profile on the boundary layer and on the velocity profile at the rotor inlet, as well as of optimizing this profile. A simplified axisymmetric steady flow model has been defined by neglecting the influence of the inducer on the inlet flow; as well, the shaft rotation has been neglected. Consequently, the axial part of the inlet nozzle has been extended three diameters ($180mm$) downstream of the rotor inlet section. A constant outlet pressure, $p_u = 0.93atm$, has been imposed at this section, far downstream of the section of interest (refer to Fig. 1). The imposed pressure value corresponds to high-load working conditions of the Pegasus engine. The external intake diameter is $D_e = 57.3\ mm$, whereas the shaft diameter is $D_i = 18\ mm$. The rotor-shaft blind nut is represented by an elliptical arc with semi-axes $a = 6mm$ and $b = 9\ mm$. The shaft has been considered as a fixed solid boundary. The computational domain has been extended slightly upstream of the intake inlet, by empirically defining an inlet surface with enforced normal direction of the velocity vector and ambient total conditions ($p_0 = 1atm$, $T_0 = 293K$). This axisymmetric geometry has been discretized by means of a structured grid with 8432 cells (refer to Fig. 1). The compressible, turbulent, steady, axisymmetric flow has been computed by means of the CFD code FLUENT©, version 6.1.18 [Flu-

ent 6.1 Inc. (2003)], using a three-level full-multigrid technique to accelerate convergence to steady state.

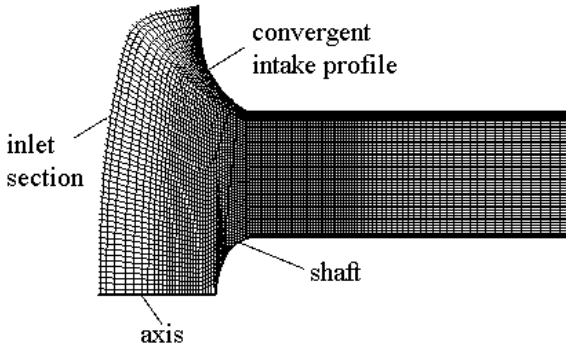

Figure 1: Computational structured grid for the simplified intake geometry.

Fig. 2 shows the axial shear stress distribution on the outer wall, computed using three well-known turbulence models. The three shear stress distributions are very similar to each other: all of them show that separation occurs immediately downstream of the corner between the convergent duct and the axial one. The corresponding recirculation bubble is clearly shown in Fig. 3, which provides the streamlines computed using the Spalart-Allmaras turbulence model.

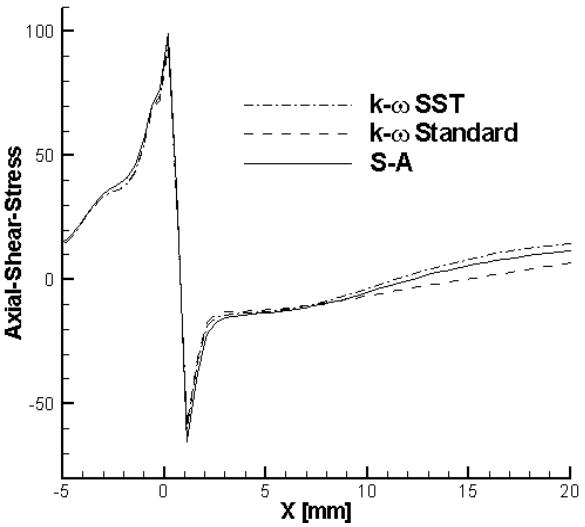

Figure 2: Axial shear stress on the outer wall computed with different turbulence models.

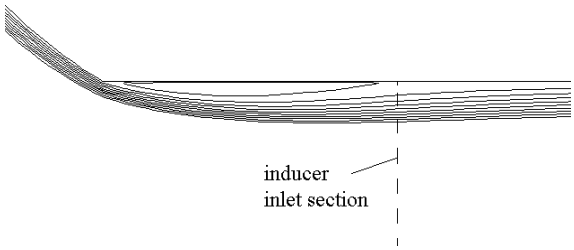

Figure 3: Zoom of the streamlines (Spalart-Allmaras turbulence model).

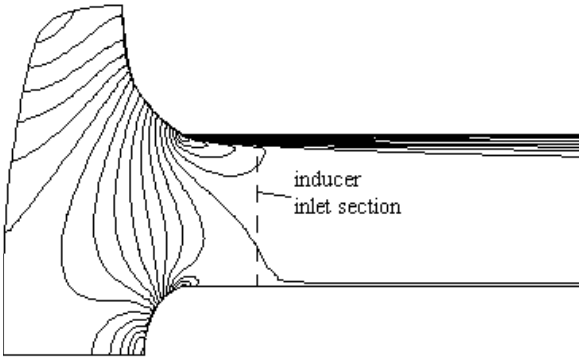

Figure 4: Mach-number contours (Spalart-Allmaras turbulence model).

The re-attachment occurs sufficiently ahead of the inducer inlet section, denoted by a dashed line, thus proving the hypothesis of neglecting the influence of the inducer blades to be realistic. The low total-pressure flow region downstream of the recirculation bubble significantly perturbs the velocity profile at the inducer inlet, as shown by the Mach-number contours provided in Fig. 4. Correspondingly, the relative velocity profile becomes skew at the blade tip, where no additional twisting has been provided by the manufacturer to compensate this effect. This low total-pressure flow affects approximately 8% of the rotor inlet section, causing also a reduction of the mass flow rate. These arguments suggest to re-define the intake profile with the aim of eliminating the recirculation bubble and of reducing the boundary-layer growth. This goal requires a numerical design optimization technique, since the simpler strategy of choosing a *reasonable* smooth profile does not guarantee suitable operating conditions, as it will be shown in Section 3.1.

3 Progressive optimization technique

A general methodology to optimize the described configuration, as well as other fluid-dynamic components, is proposed in this section. Its starting point is the progressive optimization technique presented in [Dadone and Grossman (2000)] and applied to the design of ducts, airfoils and cascades. However, the adjoint method of Dadone and Grossman (2000) does not allow the use of black-box analysis codes, since the source code needed to derive the adjoint system is not available. Incidentally, even if the source code were available, the derivation of the adjoint system would be very cumbersome for equations including turbulence. Thus, the adjoint formulation has been here replaced by a finite-difference approach. This increases the computational work required to find out the optimal solution. The computational work is also affected by the number of design variables. Indeed, for each global step of the optimization process, one (not fully converged) computation of the flow field is required for each perturbed design parameter in order to evaluate the corresponding sensitivity derivative. Nevertheless, the very high efficiency due to the simultaneous convergence of the flow solution and of the optimization process, as well as to the use of different grid levels, is retained. Moreover, this approach can be combined with all commercial black-box codes currently used for the analysis of engineering systems and components.

After defining the objective function, I, its minimum value can be efficiently found as follows:

(1) fix an initial vector of n design variables, $\xi^0 = \left(\xi_1^0, ..., \xi_n^0\right)$, which define the intake profile;

(2) start the flow computations on a coarse grid;

(3) advance the flow solver for several iterations and compute the objective function, I^ℓ;

(4) add a small increment, $\Delta\xi_i$, to the value of each design parameter and perturb the grid; using a restart solution, compute the flow with the same convergence level, and evaluate the objective function, I_i^ℓ;

(5) compute the objective function gradient by means of finite differences:

$$\frac{\partial I}{\partial \xi_i} = \frac{I_i^\ell - I^\ell}{\Delta\xi_i}, \quad i = 1, \ldots, n; \tag{1}$$

(6) update the design variables according to the relation:

$$\xi_i^{\ell+1} = \xi_i^\ell - a_i \frac{\partial I}{\partial \xi_i}, \quad i = 1, \ldots, n, \tag{2}$$

where a_i are positive parameters;

(7) repeat steps 3 to 6 until the norm of the objective function gradient is sufficiently reduced;

(8) refine the mesh;

(9) repeat steps 3 to 6 until the norm of the objective function gradient is further reduced;

(10) repeat steps 8 and 9 until the finest grid level is reached;

(11) repeat steps 3 to 6 until the objective function gradient becomes sufficiently small.

The coefficients a_i in Eq. (2) are evaluated as:

$$a_i = \frac{\Delta\xi_c}{k\,|\nabla_i I|^0_{max}} c_i, \quad i = 1, \ldots, n. \tag{3}$$

In Eq. (3), $\Delta\xi_c$ is the typical change of the design variables, $k$is a coefficient which can vary from 40 to 100 accordingly to the considered application, and finally $|\nabla_i I|^0_{\max}$ is the largest absolute value of the sensitivity derivatives computed at the first global step of the optimization process. The amplification factor, c_i, varies from a minimum value equal to 1 to a maximum value, c_M, which depends on ∇I. Normalizing the gradient at the ℓ^{th} iteration as

$$r = \log \frac{|\nabla I|^0}{|\nabla I|^\ell}, \tag{4}$$

c_M is set to 10 if r is less than 1, to 40 if r is greater than 2, whereas it varies linearly between 10 and 40 for intermediate values of the considered ratio. At the beginning of the process c_i is equal to 1; then it is increased by 50% if the corresponding

sensitivity derivative maintains its sign, otherwise it is decreased by 50%. This approach performs better than the steepest descent method, corresponding to c_i equal to 1. Indeed, large changes are applied to the design variables whose sensitivity derivates maintain their sign, while small variations are assigned to the design parameters whose sensitivity derivatives are changing their sign.

The flow solver convergence level decreases progressively according to the mesh level and to ∇I, so as to increase the accuracy of the objective function computation, while approaching the optimal solution. Thus the initial configurations, which differ considerably from the optimized one, are analyzed at a very low computational cost: indeed, the sole aim of the first analyses is to find out an approximate direction in the design space, leading to the reduction of the objective function.

In order to further increase the efficiency of the presented strategy, the mesh is generated completely only a few times throughout the overall optimization process. In all other cases, the position of the mesh nodes is updated using a grid perturbation technique. Accordingly, the last computed flow solution can be used as the starting solution for the next flow computation. Taking into account the distance,s_j, between the mesh nodes and the nearest boundary node, the mesh node position has been perturbed as follows [Marocco (1984), Medic, Mohammadi, Petruzzelli, Stanciu and Hecht (1999)]:

$$\delta s_j = \frac{1}{\int_\Gamma \frac{d\gamma}{s_j^\beta}} \int_\Gamma \frac{\delta s_w}{s_j^\beta} d\gamma, \tag{5}$$

where both integrals are extended over the solid boundaries Γ, δs_w is the displacement of each node located at the wall and $\beta \geq 2$.

In the proposed design applications, one coarse and two locally refined grid levels have been used. In all cases, the two mesh refinements have been performed when the conditions $r > 1$ and $r > 1.5$, respectively, have been maintained for three consecutive iterations of the optimization process. Furthermore, the objective function has been considered sufficiently reduced, when $r > 3$.

4 Optimization results

First, the optimization strategy has been tested versus an inverse-design problem to assess its computational efficiency. A target flow solution has been generated by analyzing a known configuration. The optimization process has been started using a set of design variables significantly different from the target one. Hence, the aim of the numerical test is to verify that the optimization technique is able to recover the target configuration in the amount of computational time to perform few flow analyses. Then the above technique has been applied to the design optimization of the intake, with the aims of cancelling the recirculation bubble and of reducing the boundary-layer growth. Using a geometrically constrained profile, two applications have been first considered, which differ in the definition of the objective function. The first application aims at minimizing the difference between the Mach number distribution computed in the rotor inlet section and the Mach number value computed using a one-dimensional isentropic flow assumption; the second application aims at maximizing the kinetic energy at the rotor inlet section, *i.e.*, at reducing the fluid-dynamic losses. In order to validate the employed single-point optimization approach, the design procedure has been repeated in off-design flow conditions, namely by imposing a different outlet pressure, *i.e.*, a different flow rate. Finally, the design optimization has been repeated after removing one geometrical constraint.

4.1 Validation test

The aim of this validation test is to check that the procedure is able to drive an arbitrary initial profile to the (known) target one, in the amount of computational time to perform few flow analyses of the reference shape, namely with the efficiency characterizing other procedures, *i.e.*, the progressive adjoint procedure of Dadone and Grossman (2000).

The target shape, denoted by a solid line in Fig. 5, corresponds to predefined values of the design parameters ξ_i, and is used to compute a target pressure distribution, $\widehat{p}_j$, that must be matched by the

pressure distribution p_j, corresponding to the current trial shape. Accordingly, the objective function is defined as:

$$I(\xi) = \frac{1}{2N} \sum_{j=1}^{N} (p_j - \widehat{p}_j)^2 \tag{6}$$

where N is the number of control points ($N = 50$) chosen on the control surface which defines the outer wall. Five design variables have been employed, the intake profile $y(x)$ being represented by the fifth-order polynomial

$$y = \xi_1 x^5 + \xi_2 x^4 + \xi_3 x^3 + \xi_4 x^2 + \xi_5 x \tag{7}$$

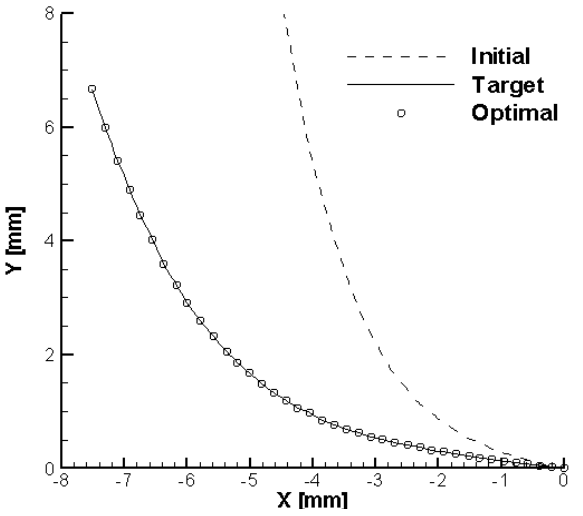

Figure 5: Inverse design. Target, initial and optimal profiles.

The initial and target pressure distributions on the outer wall are provided in Fig. 6 as dashed and solid lines, respectively. It is noteworthy that, despite the smoothness of this *reasonable* target profile, the target pressure distribution is far from representing a suitable intake pressure distribution, since the overexpansion at the corner and the final recompression are interposed by a weak recompression and a further weak expansion. This complex pressure distribution also makes the inverse design optimization a difficult task.

Fig. 7 provides the convergence histories of the logarithms of the objective function, $\log_{10}(I/I_0)$,

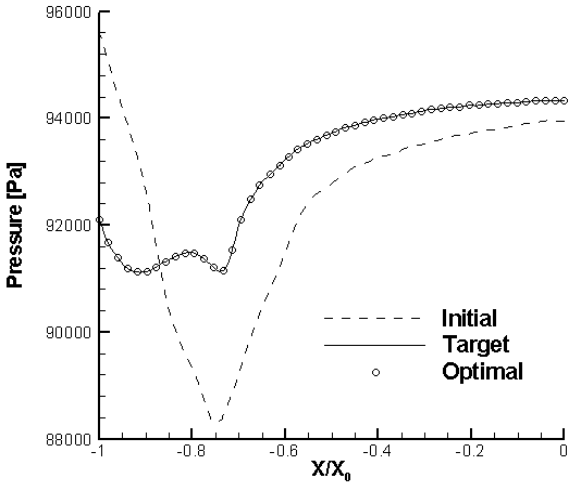

Figure 6: Inverse design. Target, initial and optimal pressure distributions.

and of the magnitude of the normalized gradient of the objective function, $\log_{10}(|\nabla I|/|\nabla I|_0)$. The abscissa in Fig. 7 is the required work, with a unit of work considered as the computational time to run a single analysis solution to convergence on the finest mesh.

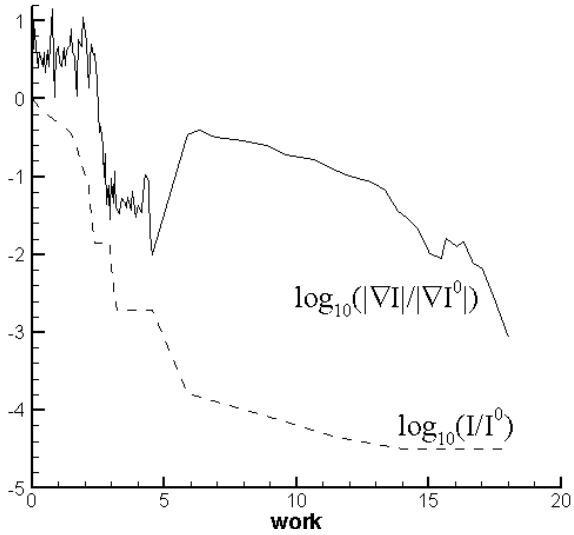

Figure 7: Inverse design. Convergence histories.

A large step towards the optimal solution is performed at the coarser grid levels at a low cost. Indeed, the mesh has been refined at *work* $\approx$ *3* and at *work* $\approx$ *4.7*, whereas the entire optimization process has required about 18 work units.

Fig. 5 shows that the optimal shape (symbols) is perfectly superposed to the target configuration (solid line). Similarly, Fig. 6 proves that the optimal pressure distribution accurately matches the target pressure distribution.

4.2 Intake profile optimization

This subsection aims at improving the turbojet performance by optimizing the intake profile.

The overall dimensions of the original intake have been retained, *i.e.*, its length and external radius have been kept constant. At this stage, also the corner between the convergent duct and the axial one is maintained in the original position. This condition reduces the number of design parameters, thus modifying Eq. (7) as follows:

$$y = \xi_1 x^5 + \xi_2 x^4 + \xi_3 x^3 + a_4 x^2 + \xi_5 x \tag{8}$$

a_4 being the value which allows to enforce the outlined geometrical constraint.

Two different definitions of the objective function have been considered, both of them aiming at reducing, or even cancelling, the recirculation bubble presented in Fig. 3, as well as at improving the velocity profile at the inducer inlet. In particular, the first definition aims at minimizing the difference between the computed Mach number distribution in the inducer inlet section and the Mach number value that would be computed using a one-dimensional isentropic flow assumption. The corresponding objective function is defined as:

$$I = \frac{1}{2 \cdot N} \sum_{j=1}^{N} \left(M_j - \hat{M}_{is} \right)^2 \tag{9}$$

In Eq. (9),N is the number of nodes ($N = 69$) on the inducer inlet section, M_j is the computed Mach number in the j^{th} node, and $\hat{M}_{is}$ is the one-dimensional isentropic Mach number ($\hat{M}_{is} = 0.324$). The boundary conditions used to compute the results plotted in Figs. 3 and 4 have been used. Moreover, the Spalart-Allmaras turbulence model has been used to compute the turbulent flow in the intake.

The original profile, denoted by a dot-dashed line in Fig. 8, is taken as initial profile of this design optimization, as well as of the following one.

Fig. 9 shows the Mach number contours computed with the optimized intake profile, provided in Fig. 8 as dashed line. This figure proves that the separation bubble has been eliminated and that at the outer wall a gradual recompression takes place, as demonstrated by the reduced boundary layer growth. The mass flow rate increases 2% with respect to the original intake.

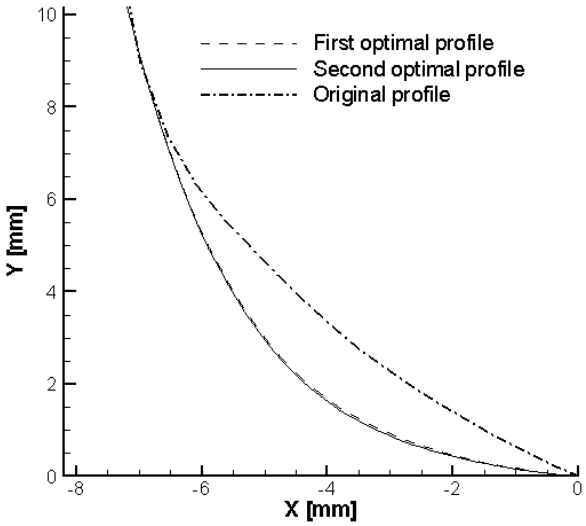

Figure 8: Comparison between the two optimal profiles with fixed corner.

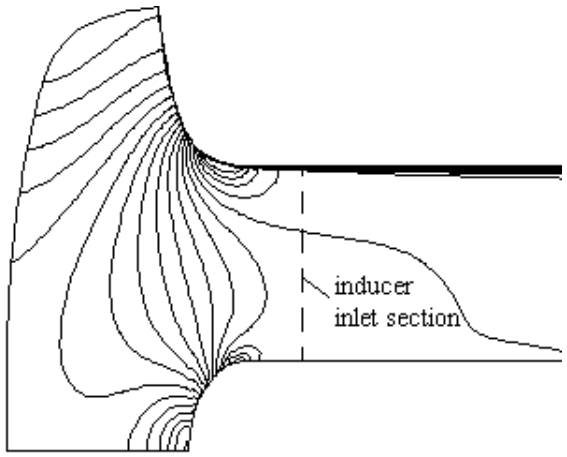

Figure 9: First design optimization. Mach number contours of the flow for the optimal intake configuration.

Fig. 10 shows the convergence histories of the ob-

jective function and of its gradient. The two grid refinements have been performed at *work* $\approx$ *0.14* and at *work* $\approx$ *4* respectively whereas the entire optimization process has required approximately 9 work units.

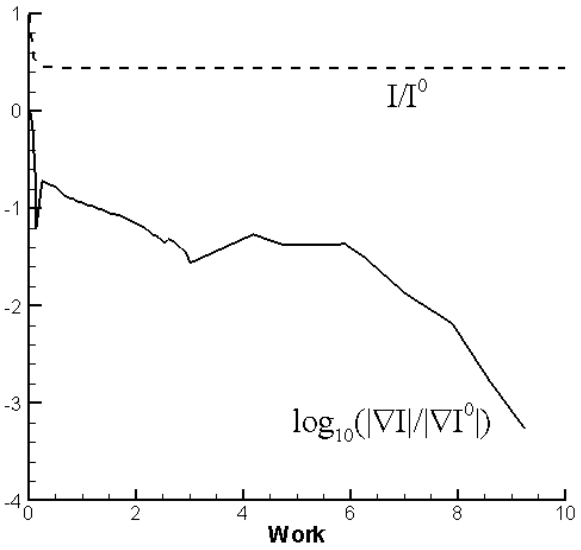

Figure 10: First design optimization. Convergence histories.

The second design optimization aims at reducing the fluid-dynamic losses, *i.e.*, at maximizing the flow kinetic energy at the inducer inlet section. The corresponding objective function to be maximized is:

$$I = \frac{1}{2}\sum_{j=1}^{N-1} \dot{m}_a v_j^2 \tag{10}$$

where v_j and $\dot{m}_a$ are the velocity and the mass flow rate in the center of the j^{th} element of the inducer inlet section.

Fig. 8 also shows the optimal intake profile (solid line) resulting from this second application, which practically coincides with the previous optimized profile. Correspondingly, also the Mach number contours are very similar to the previous contours and thus they are omitted for brevity. On the contrary, both optimal profiles significantly differ from the original one. Fig. 11 shows the convergence histories of the objective function and of its gradient. The two grid refinements have been performed at *work* $\approx$ *0.2* and *work* $\approx$ *2*, respectively whereas the entire optimization process has required approximately 9 work units.

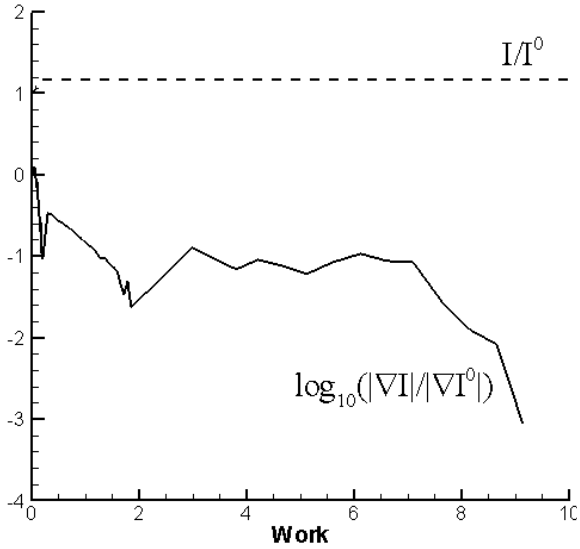

Figure 11: Second design optimization. Convergence histories.

Figs. 12 and 13 provide the Mach-number distributions and the total pressure distributions at the inducer inlet section corresponding to the two optimal profiles and to the original one. The two optimal distributions are superposed and are denoted by solid lines, whereas the dashed line refers to the original intake. Both figures remark the flow rate increase and the loss reduction. It is noteworthy that the optimal inlet velocity profile is slightly flatter than the initial one. In the design optimizations to follow, only the second objective function and the corresponding optimal profile and flow solution will be considered.

In order to check the off-design behaviour of the optimal intake profile, a new single-point design optimization has been performed, with a lower downstream pressure, $p_u = 0.88atm$. Note that the pressure reduction implies higher values of the engine rotation and of the flow rate. The intake profile optimized for the new operating conditions (which are even out of the operating range of the turbojet engine) is plotted in Fig. 15 (solid line) together with the previous optimal intake (dashed line) and the original intake profile (dot-dashed

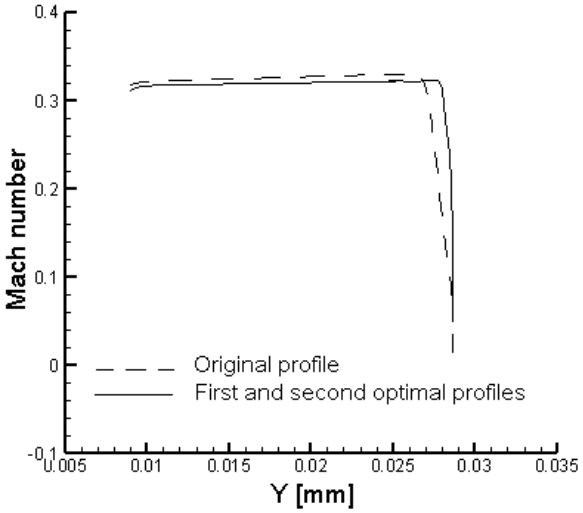

Figure 12: Design optimization with fixed corner. Mach-number distributions at the inducer inlet section.

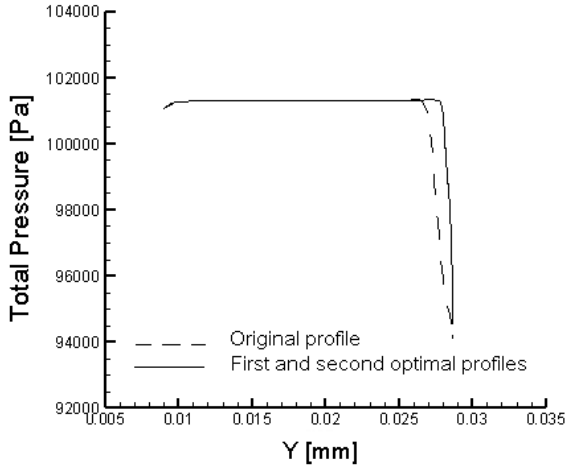

Figure 13: Design optimization with fixed corner. Total pressure distributions at the inducer inlet section.

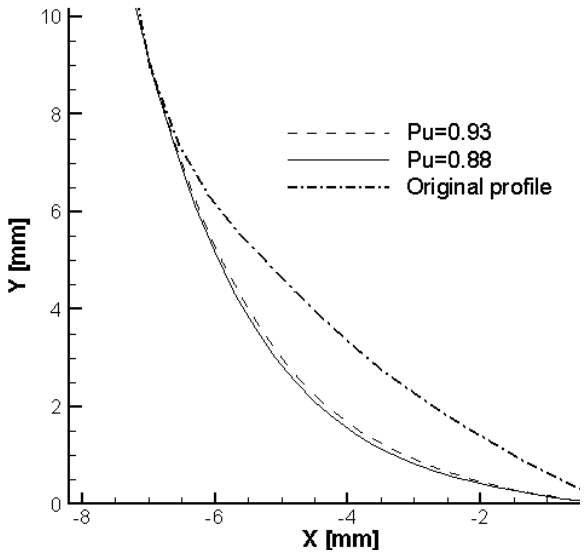

Figure 14: First design optimization. Optimal intake profiles under different operating conditions.

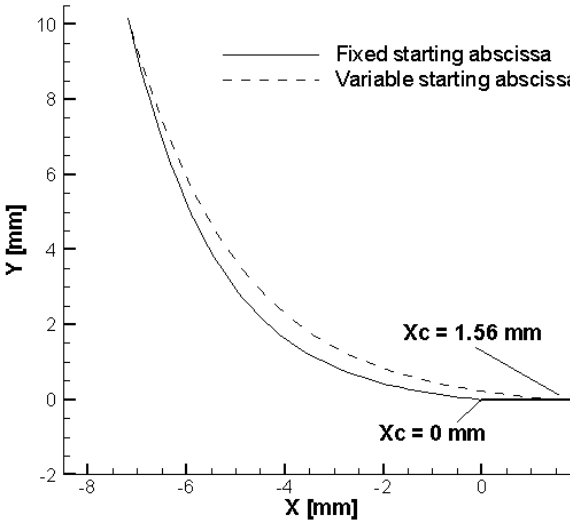

Figure 15: Comparison between the optimal profiles with fixed and variable starting abscissa.

line).

The two optimal profiles are very close, thus demonstrating that the design optimization is not very sensitive to a variation of the operation conditions. This conclusion proves that this design application can be afforded by the simple single-point design strategy here employed. Similar results have been obtained enforcing a higher downstream pressure, $p_u = 0.96atm$, *i.e.*, for lower values of the engine regime and of the flow rate.

In the previous design applications, the corner between the convergent duct and the axial part of the duct has been preserved in the original location. In the final design optimization here considered, the corner point is allowed to move axially; correspondingly, its abscissa x_c can assume non-zero values. Thus, the intake profile is represented by

the following equation:

$$y = \xi_1(x-x_c)^5 + \xi_2(x-x_c)^4 + +\xi_3(x-x_c)^3 + a_4(x-x_c)^2 + \xi_5(x-x_c) \quad (11)$$

In Eq. (11), ξ_1, ξ_2, ξ_3, ξ_5, and x_c are the five design parameters. The previous reference operating conditions have been imposed, *i.e.*, $p_0 = 1atm$, $T_0 = 293K$ at inlet, $p_u = 0.93atm$ at outlet. The computed optimal intake profile with variable initial abscissa of the convergent duct, x_c, is represented in Fig. 15, together with the previous optimal profile corresponding to fixed initial abscissa, $x_c = 0$. The computed optimal initial abscissa is $x_c = 1.56$. The resulting profiles appear significantly different. Nevertheless, the present optimal intake determines a negligible further increase of the mass flow-rate, *i.e.*, 0.1% for $p_u = 0.93atm$ and 0.3% for $p_u = 0.88atm$.

The results computed for different operating conditions are summarized in Tab. 1. The convergence histories of the present design optimization are plotted in Fig. 16, which underlines that the variation of the initial abscissa, x_c, determines a reduction of the optimization efficiency. Indeed, 25 work units are required to decrease the gradient of the objective function three orders of magnitude. The two grid refinements have been performed at *work* $\approx$ *0.2* and *work* $\approx$ *1.4*, respectively.

Table 1: Mass flow-rate for the original and the optimal profiles for different operating conditions.

	Mass flow rate [g/s]		
downstream pressure $p_u[atm]$	PEGASUS Mk3 original profile	optimal profile ($x_c = 0$)	optimal profile ($x_c \neq 0$)
0.88	354.9	363.1	364.1
0.93	279.8	285.9	286.2
0.96	215.3	220.0	220.0

5 Experimental validation

Fig. 17 shows an overall view of the experimental rig which has been set up to test the small-scale turbojet engine. The microturbine assembly has undergone some modifications to allow control and data acquisition by means of an external PC. In particular, the original fuel tank has been substituted by a new tank (3), which has been hanged up in order to measure the fuel flow rate by means of a load cell (6). The fuel consumption is evaluated as the difference of two weightings within a 1 minute period of steady operating conditions, the measurement range of the load cell being 0÷30 N, and the measuring error being 1% of the full scale. The turbojet is suspended on a parallelogram (5) to measure the axial and the lateral components of the thrust. In particular, the axial thrust is measured by means of two load cells (4) with a measurement range of 0÷120 N, whereas the undesired lateral thrust is measured by means of a load cell (2) with a range of 0÷60 N. The rotational speed is measured by a pick-up (1) mounted on the compressor outer case and facing the inducer blades. A data acquisition system allows to display and to record all measured quantities.

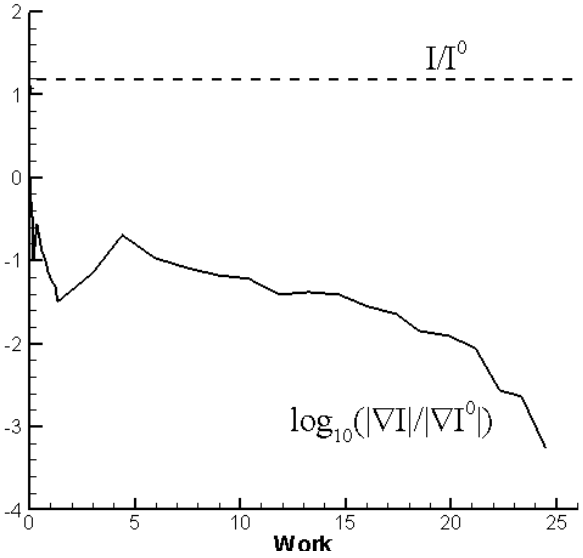

Figure 16: Design optimization with variable initial abscissa, x_c. Convergence histories.

First, the Pegasus turbojet engine has been equipped with the original intake. Then, the optimal profile provided by the third design optimization has been tested. Both configurations have been experimentally tested under the same ambient conditions, to assess the real effects of the pro-

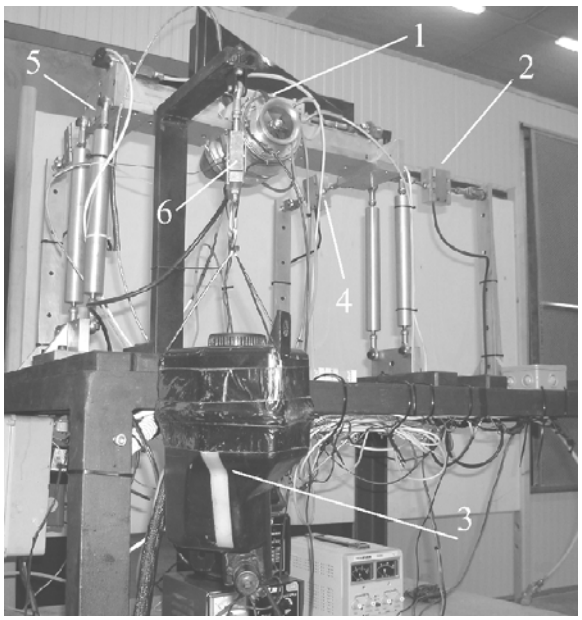

Figure 17: Overall view of the Pegasus turbojet test bed: 1) pick up, 2) side load cell, 3) fuel tank, 4) one of the two rear load cells, 5) parallelogram, 6) fuel load cell.

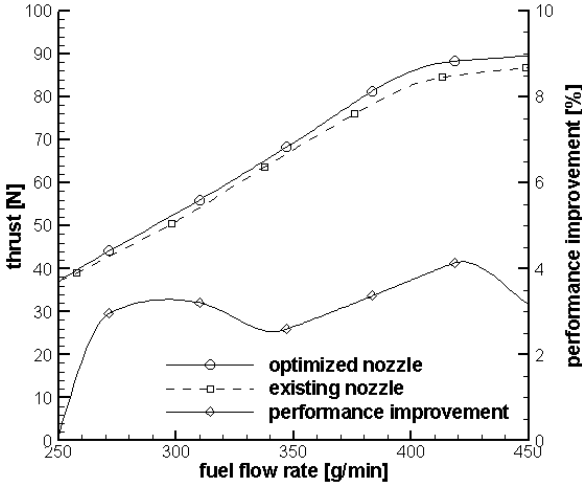

Figure 18: Thrust measurements for the existing and the optimal nozzles.

posed simplified design optimization of the intake on the overall performances of the turbojet engine. Fig. 18 shows the thrust versus the fuel flow rate for the two configurations. The performance improvement due to the optimal intake profile is also plotted. Fig. 18 underlines that optimal profile provides a performance improvement ranging from 3% to 4%. This performance improvement can be considered fully satisfactory, since only one turbojet component has been analyzed and optimized.

As shown in Section 4, the optimal intake is characterized by a mass flow rate 2-3% higher than the mass flow rate of the original intake. Alternatively, for the same mass flow rate, the optimal profile is characterized by a higher pressure at the inducer inlet with respect to the original intake, *i.e.*, by a higher global compression ratio and accordingly by an increased thermal (conversion) efficiency. Moreover, the improved inlet velocity profile limits the pressure losses at the tip of the inducer blades. Fig. 18 also underlines that the benefits of using a re-designed intake profile vanish at low-load conditions. Indeed, at small mass flow rate and rotational speed, the intake final recompression is weak and the recirculation bubble characterizing the original intake disappears.

6 Conclusions

A small-scale Pegasus turbojet engine has been analyzed. A simplified, rotor-free, numerical simulation of the flow in the intake has revealed a boundary-layer separation immediately downstream of the sharp corner between the convergent intake portion and the axial duct. The presence of a recirculation bubble reduces the inducer inlet velocity in 8% of the rotor inlet section and determines a 2-3% reduction of the mass flow rate. Further numerical computations have shown that the choice of a *reasonable* smooth profile is not sufficient to guarantee suitable intake operation conditions. Therefore, a gradient-based progressive optimization procedure appropriate to be used in combination with black-box simulation codes has been developed to re-design the intake profile. The efficiency of the proposed optimization technique comes from the simultaneous convergence of the flow solution and of the optimization process, as well as from the use of nested grid levels. Moreover, the finite-difference sensitivities are computed by means of partially converged flow solutions. The proposed design optimization strategy can be straightforwardly applied to all en-

gineering fields which employ commercial black-box codes as simulation tools.

An inverse design application with known optimal solution has been preliminarily considered to validate the robustness and the efficiency of the optimization technique. In this application, the proposed optimization strategy has reduced the magnitude of the gradient of the objective function by three orders of magnitude in the amount of computational work to perform 18 flow analyses. Then, two single-point optimizations suitable for the design of the rotor-free intake have been defined. The first one is an inverse design with prescribed Mach number at the rotor inlet section, whereas the second optimization requires the maximization of the kinetic energy at the inducer inlet section. Both design optimizations aim at reducing the pressure losses, namely at cancelling the recirculation bubble and at reducing the boundary-layer growth. During these optimizations, the location of the point connecting the convergent and the axial portions of the intake has been maintained fixed. The two resulting optimal intake profiles are almost coincident and produce a 2% increase of the mass flow rate, together with a significant improvement of the velocity profile at the inducer inlet section. Note that these improvements are due to the elimination of the recirculation bubble. Both design optimizations have been produced in the amount of computational work to perform 9 flow analyses. Almost coincident intake profiles and performance improvements have been obtained by re-designing the intake profile for higher (+25%) and lower (-25%) mass flow rates, thus suggesting that the design optimization of a small-scale turbojet intake does not require a multi-point optimization formulation.

The last design optimization of the intake has been performed by allowing the abscissa of the point connecting the two parts of the intake to change. The resulting intake profile is significantly different from the previous ones but performs only slightly better. Indeed, the profiles with fixed connecting point have already succeeded in cancelling the recirculation bubble, and the unique possible improvement is the reduction of the axial extension of the final recompression region to limit the boundary-layer growth ahead of the rotor inlet. This is achieved by shifting the connecting point closer to the inducer. The negative outcome is the increase of the computational time to the amount required to perform 25 flow analyses.

Finally, an experimental rig has been set up to test the performance improvements of the turbojet engine, obtained by re-designing the intake. For most of the operating range, the optimal profile provides a performance improvement ranging from 3 to 4%, on account of the slightly increased global compression ratio and of the improved inlet velocity profile, which limits the pressure losses at the tip of the inducer blades. This performance improvement can be considered fully satisfactory, since only one component has been analyzed and optimized.

We can conclude that the proposed progressive optimization technique for black-box simulation codes is capable of producing a rather complex design optimization in an amount of computational work which is acceptable for engineering applications. Moreover, the experimental tests allow to state that the design optimization of the intake of a small-scale microturbine can be afforded using simplified geometry and flow model.

References

Carno, J. et al. (1998): Micro gas turbine for combined heat and power in distributed generation. *ASME 98-GT-309*.

Dadone, A.; Grossman, B. (2000): Progressive Optimization of Inverse Fluid Dynamic Design Problems. *Computers and Fluids*, vol. 29, no. 1, pp. 1-32.

Decuyepere, R.; Verstraete, D. (2005): Microturbines from the standpoint of potential users. *VKI LS on micro gas turbines*.

Fernandez-Pello, A.C. (2005): Micro-power using combustion: issues and approaches. 29^{th} *symposium on combustion*, Japan.

Fluent 6.1 Inc. (2003), Fluent Europe users guide: vol. 1-4.

Guidez, J.; Dumand, C.; Courvoisier, T.; Orain, M. (2005) Specific Problems of Micro Gas Turbine for Micro Drones Application. *ISABE Paper 2005-1273*.

Guidez, J.; Ribaud, Y.; Dessornes, O; Dumand, C. (2004): Micro engines for microdrones propulsion. 4^{th} *European Micro UAV Meeting*, Toulouse.

Hamilton, S.L. (1999): Microturbines poised to go commercial. *Modern power systems*, vol. 19, no. 9, pp. 21-22.

Hendrik, P.; Verstraete, P.; De Bruyn, N. (2004): An ultra micro gas turbine intended for MAV propulsion. 7^{th} *International UAV conference*, Bristol.

Jacobson, S.A. (1998): Aerothermal challenges in the design of a microfabricated gas turbine engine. *AIAA Paper 98-2545*.

Marocco, A. (1984): Simulations Numeriques dans la fabrication des circuits à semiconducteurs (process modelling). *RR 035*, INRIA, France.

McDonald, C.F. (1996): Heat recovery exchanger technology for very small gas turbines. *International Journal of Turbo and Jet Engines*, vol. 13, pp. 239-261.

Medic, G.; Mohammadi, B.; Petruzzelli, N.; Stanciu, M.; Hecht, F. (1999): 3D Optimal Shape Design for Complex Flows: Application to turbomachinery. *AIAA Paper 99-0833*.

Morino L.; Bernardini G.; Mastroddi F. (2006): Multi-disciplinary optimization for the conceptual design of innovative aircraft configurations. *CMES: Computer modeling in Engineering & Sciences*, Vol. 13, No. 1, pp. 1-18.

P 'ascoa, J.C.; Mendes A.C.; Gato, L.M.C.; Elder R. (2004): Aerodynamic design of turbomachinery cascades using an enhanced time-marching finite volume method. *CMES: Computer modeling in Engineering & Sciences*, Vol. 6, No. 6, pp. 537-546.

Poloni, C.; Giurgevich, A.; Onesti, L.; Pediroda, V. (2000): Hybridization of a multi-objective genetic algorithm, a neural network and a classical optimizer for a complex design problem in fluid dynamics. *Comput. Methods Appl. Mech. Engrg.*, vol. 186, pp. 403-420.

Rama Mohan Rao A.; Appa Rao T.V.S.R.; Dattaguru B. (2004): Generating optimised partitions for parallel finite element computations employing float-encoded genetic algorithms. *CMES: Computer modeling in Engineering & Sciences*, Vol. 5, No. 3, pp. 213-234.

Rodgers, C. (1999): 25-5 Kwe Microturbine Design Aspects. *ASME 2000-GT-0626*.

Rodgers, C. (1997): Thermo-Economics of a small 50 kW Turbogenerator. ASME 97-GT-260.

Waitz, I.A.; Gauba, G.T.; Tzeng, Y.S. (1998): Combustor for Micro-Gas Turbine Engines. *Journal of Fluid Engineering*, vol. 120, pp. 109-117.

Watts, J.H. (1999): Microturbines: a new class of gas turbine engine. *Global gas turbine news*, vol. 39, no. 1,
pp. 4-8.

Zhu, Z.Q.; Liu Z.; Wang, X.L.; Yu R.X. (2004): Construction of integral objective function/fitness function of multi-objective/multi-disciplinary optimization. *CMES: Computer modeling in Engineering & Sciences*, Vol. 6, No. 6, pp. 567-576.